PA Recon

David Fuentes

April 12, 2015

The presence of deoxyhemoglobin PA signal provides a biomarker for locating aggressive prostate cancer. Spectral unmixing to differentiate deoxy- (HHb) and oxyhemoglobin (HbO2) PA signal is achieved using inverse analysis applied to physics based models of the reconstruction. Modeling the reconstruction involves: (Section 2) estimating the initial pressure distribution from the absorbed light source and (Section 3) propagating the acoustic wave from the initial pressure distribution to the ultrasound receiver hardware. An information theoretic mathematical framework for adaptive sampling and identifying wavelength and SNR acquistion parameters that provide the most information content with respect to the physics model based data collection is presented in Section 1. The MATLAB script `exampleRecon.m` documents the user interface developed, Section 4. The interface allows the operator to denote needle insertion points within the global DICOM frame. GPU kernels are provided for compute intensive elements of the pipeline to enable high throughput processing.

Tradeoffs between accuracy in the physics based predictions and numerical efficiency are considered within the context of the model-based reconstruction. A key idea of our approach is that clinically significant spatial variations of sO2 may be detected using the appropriate numerical approximations. Ie, full numerical solution to the coupled partial differential equations that govern the inherent fluence and pressure for photoacoustic detection are not needed.

1 Mathematical Framework

The underlying philosophy and assumptions within our approach is that the physics models are 1st order accurate or within 70-80% of the needed accuracy and the error is adequate within the assumed Gaussian noise. Gaussian distributions provide analytical representations of the random variables of interest (ie volume fraction of HHb, ϕ) within the Bayesian setting and provide a crux for understanding. In particular, we say that a random variable η belongs to a multi-variate normal distribution of mean $\mu \in \mathbb{R}^n$ and covariance $\Sigma \in \mathbb{R}^{n\times n}$

$$\eta \sim \mathcal{N}(\mu, \Sigma) \Rightarrow p(\eta) = \frac{1}{2\ \pi\ \det \Sigma} \exp\left(-\frac{1}{2}\|\mu - \eta\|^2_\Sigma\right)$$

1. Our data acquistion model, $\mathcal{G}(\vec{k}, \theta) : \mathbb{R}^a \times \mathbb{R}^m \to \mathbb{R}^n$, maps deterministic acquisition parameters, $\vec{k} \in \mathbb{R}^a$, and uncertain parameters, $\theta \in \mathbb{R}^m$ to observables, $\vec{z} \in \mathbb{R}^n$ (or $\vec{z} \in \mathbb{C}^n$). Explicitly, we will assume that the measurement models are corrupted by zero mean white noise noise of a **known** covariance matrix, $\Sigma_z \in \mathbb{R}^{n\times n}$

$$\begin{aligned} \vec{z} &= \mathcal{G}(\vec{k}; \theta) + \eta \qquad \eta \sim \mathcal{N}(0, \Sigma_z) \\ \vec{k} &= \text{(frequency, laser position, etc)} \\ \theta &= \text{(volume fraction, absorption, etc)} \end{aligned} \tag{1}$$

   η may be interpreted as the measurement noise or the acquisition noise in the sensor model. For a deterministic measurement model $\mathcal{G}$, the conditional probablity distribution has an explicit analytical form and may be written as a **known** Gaussian distribution.

$$p(\vec{z}|\theta) = \mathcal{N}(\mathcal{G}(\vec{k}; \theta), \Sigma_z)$$

2. Additional **known** information is the prior probability distributions for the model parameters, $p(\theta)$. For simplicity, assume that Prior parameters are Gaussian distributed of **known** mean, $\hat{\theta}$ and covariance, Σ_θ

$$\theta \sim \mathcal{N}(\hat{\theta}, \Sigma_\theta)$$

3. Bayes theorem is fundamental to the approach. The probability of the measurements $p(z)$ must be interprited in terms of the known information. The probability of the measurements may be derived from the marginalization of the joint probability and has the interpretation as the projection of the joint probability onto the measurement axis.

$$p(z) = \int_\theta p(\theta, z)\ d\theta = \int_\theta p(z|\theta)\ p(\theta)\ d\theta$$

4. The concept of informational entropy [Madankan et al., 2015], $H(Z)$, provides a mathematically rigorous framework to look for measurement acquisition parameters, $\vec{k}$, with the high information content of the reconstruction. Given a probability space $(\Omega, \mathcal{F}, p)$ (probability maps from the sigma-algebra of possible events $p : \mathcal{F} \to [0, 1]$ sigma-algebra, $\mathcal{F}$, defined on set of 'outcomes' Ω [Durrett, 2010]), we will define information of an event as proportional to the inverse probability.

$$\text{information} \equiv \frac{1}{p(z)}$$

Intuitively, when a low probability event occurs this provides high information. The informational entropy is an *average* of the information content for a sigma algebra of events $\mathcal{F}$

$$H(Z) = \int_Z p(z) \ln \frac{1}{p(z)}\ dz \qquad p(z) = \int_\theta p(z|\theta)\ p(\theta)\ d\theta$$

Hence this entropy measure is an average of the information content for a given set of events, $\mathcal{F}$, and is proportional to the variance or uncertainty in which the set of events occur. This agrees with thermodynamic entropy; if the information containing events are completely spread out such as in a uniform distribution, the entropy is maxmized. The entropy is zero for a probability distribution in which only one event occurs. Zero information is gained when the same event always occurs ($0 \ln \frac{1}{0} = 0$). Intuitively, we want to find acquisition parameters, $\vec{k}$, for which the measurements are most uncertain

$$\max_k H(Z) \quad \Leftrightarrow \quad \min_k \int_Z dz \underbrace{\int_\theta d\theta\ p(z|\theta)\ p(\theta)}_{p(z)} \underbrace{ln\left(\int_\theta d\theta\ p(z|\theta)\ p(\theta)\right)}_{ln\ p(z)}$$

Alternatively we may consider this entropy maximization problem as a sensitivity analysis for the variance of the measurement Z, ie . $\max_k H(Z) \approx \max_k \text{Var}(Z)$

$$\bar{Z} = \mathbb{E}[Z] = \int_Z dz\ z \underbrace{\int_\theta d\theta\ p(z|\theta)\ p(\theta)}_{p(z)}$$

$$\mathbb{E}[(Z - \bar{Z})^2] = \int_Z dz\ (z - \bar{Z})^2 \underbrace{\int_\theta d\theta\ p(z|\theta)\ p(\theta)}_{p(z)}$$

$$\propto \int_Z dz\ (z - \bar{z})^2 \int_\theta d\theta \exp\left(-\frac{1}{2}\|z - \mathcal{G}(\vec{k}, \theta)\|^2_{\Sigma_z}\right) \exp\left(-\frac{1}{2}\|\theta - \hat{\theta}\|^2_{\Sigma_\theta}\right)$$

Probilistic integrals may be computed from uncertainty quantification techniques [Fahrenholtz et al., 2013].

2 Fluence Source

Reconstruction methods incorporate the spatial distribution of the absorption and scattering into the expected time dependent photo-acoustic signal of a single wavelength excitation. Diffusion-based light transport models in turbid media as well as directional models of light propagation using considerations of the delta-Eddington phase function are available [MacLellan et al., 2013, Fuentes et al., 2013, Fuentes et al., 2010, Fuentes et al., 2009]. A key idea of the inverse analysis is that the optical absorption provides the image contrast within the spectral unmixing. Within our application, the optical absorption, μ_a, is considered a linear combination of the volume fractions, ϕ, of deoxy- (HHb) and oxyhemoglobin (HbO2) constituents.

$$\mu_a(\lambda, x) = \phi(x)\mu_a^{\text{HHb}}(\lambda) + (1 - \phi(x))\mu_a^{\text{HbO2}}(\lambda)$$

Spatial variations in the optical absorption are directly related to hypoxic regions and will be detected by exploiting the frequency dependence of the optical properties. Spatial variations in optical parameters are considered as the spatial decomposition of the prostate domain, Ω

$$\Omega = \cup_j \Omega_j \qquad \Omega_i \cap \Omega_j = \emptyset \quad i \neq j \qquad \psi_j(x) = \begin{cases} 1 & x \in \Omega_j \\ 0 & x \notin \Omega_j \end{cases} \qquad \phi(x) = \sum_{j=1}^{N_\phi} \phi_j \psi_j(x)$$

Within the context of our mathematical framework, Section 1, the volume fraction mixing parameter and the optical parameters are uncertain model variables, θ. The wavelength is the deterministic acquisition parameters, $\vec{k}$. we have little information about the mixing parameter ϕ and will consider this to be uniformly distributed. Optical absorption is both species and wavelength dependent. We assume that the optical parameters is Gaussian distributed about the mean of the tabulated spectrum.

$$\phi_j \sim \mathcal{U}(0,1) \qquad \mu_a^{\mathrm{HHb}}(\lambda) \sim \mathcal{N}\left(\bar{\mu_a}^{\mathrm{HHb}}(\lambda), \Sigma_{\mu_a}\right) \qquad \mu_a^{\mathrm{HbO2}}(\lambda) \sim \mathcal{N}\left(\bar{\mu_a}^{\mathrm{HbO2}}(\lambda), \Sigma_{\mu_a}\right)$$

$$\theta = \left(\phi_1, ..., \phi_{N_\phi}, \mu_a^{\mathrm{HHb}}(\lambda), \mu_a^{\mathrm{HbO2}}(\lambda)\right) \qquad \vec{k} = \lambda$$

2.1 Standard Diffusion Approximation

The starting point for modeling light transport in tissue is the Boltzman equation for the radiance, $L(\mathbf{r}, \hat{s})$.

$$\hat{s} \cdot \nabla L(\mathbf{r}, \hat{s}) + \mu_t(\mathbf{r}) L(\mathbf{r}, \hat{s}) = \mu_s \int_{4\pi} p(\hat{s}, \hat{s}') L(\mathbf{r}, \hat{s}) \, d\omega \qquad \mu_t = \mu_a + \mu_s \tag{2}$$

Here the radiance, $L(\mathbf{r}, \hat{s})$, represents the radiant power per unit of solid angle about unit vector $\hat{s}$ and per unit area perpendicular $\hat{s}$. The Boltzman equation represents a conservation of energy applied to light energy transport in tissue at point r. The phase function, $p(\hat{s}, \hat{s}')$, provides a measure of the probability of a scattering photons traveling in direction $\hat{s}'$ into the direction $\hat{s}$. The mean cosine of the scattering angle is known as the anisotropy factor, g

$$\int_{4\pi} p(\hat{s} \cdot \hat{s}')(\hat{s} \cdot \hat{s}') d\omega' \equiv g$$

By convention, the radiance is considered as the summation of a *known* primary light source with irradiance, $E(\mathbf{r})$, traveling in direction s_0 and scattered light source.

$$L(\mathbf{r}, \hat{s}) = L_p(\mathbf{r}, \hat{s}) + L_s(\mathbf{r}, \hat{s}) = \frac{E(\mathbf{r})\delta(1 - \hat{s} \cdot \hat{s}_0)}{2\pi} + L_s(\mathbf{r}, \hat{s})$$

The scattered radiance may be represented as sum of spherical harmonics, this is known as the P-n approximation[Welch and Van G Modest, 2013].

$$L_s(\mathbf{r}, \hat{s}) = \sum_i^\infty L_i(\mathbf{r}) P_i(\hat{s})$$

When only the first two terms are used, this is known as the P-1[Modest, 2013] or diffusion approximation[Modest, 2013].

$$L_s(\mathbf{r}, \hat{s}) \approx \frac{1}{4\pi} \varphi_d(\mathbf{r}) + \frac{3}{4} \mathbf{j}(\mathbf{r}) \cdot \hat{s} \tag{3}$$

When i=0,1,2,3 terms are kept, this is known as the P-3 approximation. The P-2 approximation is generally less accurate and not used[Modest, 2013].

The diffusion model for light transport is valid under the assumption that light is scattered more than absorbed.

$$\mu_a << \mu_s(1 - g) \Rightarrow \mu_{eff} << \mu_t$$

The PDE for the SDA is obtained in two steps by (i) substituting (3) into (2) and integrating over all solid angles and (ii) multipling (2) by $\hat{s}$ and integrating over all solid angles. Combining the result yeilds

$$\nabla \cdot \left(\frac{1}{3\mu_{tr}} \nabla \varphi_d(\mathbf{r})\right) - \mu_a \varphi_d(\mathbf{r}) = -\mu_s E(\mathbf{r}) + \nabla \cdot \left(\frac{g\mu_s}{\mu_{tr}} E(\mathbf{r}) \hat{s}_0\right) \qquad \mu_s' = \mu_s(1 - g) \quad \mu_{tr} = \mu_a + \mu_s'$$

$$\mathbf{j}(\mathbf{r}) = \frac{-1}{3\mu_{tr}} \left[\nabla \varphi_d(\mathbf{r}) - 3g\mu_s E(\mathbf{r}) \hat{s}_0\right] \qquad \mu_{eff} = \sqrt{3\mu_a \mu_{tr}}$$

$\mathbf{j}$ is the radiant flux, $\hat{z}$ is the direction of the collimated light, etc...

2.2 Homogenious Coefficients

Through the diffusion model, the scattered fluence z is obtained from the known irradiance $E(x,t)$ (primary source of photons) and its flux $\mathbf{F}(x,t)$ [Fuentes et al., 2011]. The total fluence at a point is given by the sum of the scattered and primary light $\varphi_t(x,t) = z(x,t) + E(x,t)$. The irradiance is provided by a photon flux emitted throughout the domain of an interstitial laser fiber Ω_{tip}. The photons are emittied by an applied power density, $P^*\left[\frac{W}{m^3}\right]$. Each position in the domain $\hat{x} \in \Omega_{tip}$ is treated as a point source of irradiance

$$dE(x,\hat{x}) = \frac{P^*(t)d\hat{x}}{4\pi\|\mathbf{x}-\hat{\mathbf{x}}\|^2}$$

The total irradiance and flux is the integral of each attenuated point source.

$$E(x,t) = \int_{\Omega_{tip}} \frac{P^*(t)}{4\pi\|\mathbf{x}-\hat{\mathbf{x}}\|^2} \exp\left(\mu_t^*(\mathbf{x},m)\|\mathbf{x}-\hat{\mathbf{x}}\|\right) d\hat{x}$$
$$\mathbf{F}(x,t) = \int_{\Omega_{tip}} \frac{P^*(t)}{4\pi\|\mathbf{x}-\hat{\mathbf{x}}\|^2} \exp\left(\mu_t^*(\mathbf{x},m)\|\mathbf{x}-\hat{\mathbf{x}}\|\right) \frac{\mathbf{x}-\hat{\mathbf{x}}}{\|\mathbf{x}-\hat{\mathbf{x}}\|} d\hat{x}$$

$$\mu_t^*(\mathbf{x},m) = \mu_a(\mathbf{x},m) + \mu_s(\mathbf{x},m)$$

An analytic solution may be obtained by approximating the integral for the irradiance and flux as

$$E(x,t) \approx \sum_{e\in\Omega_{tip}} E_e(x,t) = \sum_{e\in\Omega_{tip}} \frac{\Delta V_e P^*(t)}{4\pi\|\mathbf{x}-\hat{\mathbf{x}}_e\|^2} \exp\left(\mu_t^*(\mathbf{x},m)\|\mathbf{x}-\hat{\mathbf{x}}_e\|\right)$$
$$\mathbf{F}(x,t) \approx \sum_{e\in\Omega_{tip}} \mathbf{F}_e(x,t) = \sum_{e\in\Omega_{tip}} \frac{\Delta V_e P^*(t)}{4\pi\|\mathbf{x}-\hat{\mathbf{x}}\|^2} \exp\left(\mu_t^*(\mathbf{x},m)\|\mathbf{x}-\hat{\mathbf{x}}\|\right) \frac{\mathbf{x}-\hat{\mathbf{x}}}{\|\mathbf{x}-\hat{\mathbf{x}}\|}$$

where ΔV_e is the volume and $\hat{\mathbf{x}}_e$ is the centroid. By linearity, each element in the discretization may be treated as an uncoupled and independent source in the light diffusion equation.

$$-\mu_a(\mathbf{x})z_e + \mu_s^*(\mathbf{x},m)E_e = \nabla\cdot\left(-\frac{\nabla z_e}{3\mu_{tr}(\mathbf{x},m)} + \frac{\mu_s^*(\mathbf{x},m)g^*}{3\mu_{tr}(\mathbf{x},m)}(\mathbf{F})_e\right) \qquad \forall e \in \Omega_{tip}$$

The fluence resulting from each element source $(\varphi_t)_e$ may be obtained from the classical isotropic point source solution [Welch and Van Gemert, 1995]. The total emanating fluence is the superposition of the element wise solutions and reduces to a volume weighted sum over the elements.

$$\varphi_t = \sum_{e\in\Omega_{tip}} P^*(t)V_e\left(\frac{3\mu_{tr}\exp(-\mu_{eff}\|\mathbf{x}-\mathbf{x}_e\|)}{4\pi\|\mathbf{x}-\mathbf{x}_e\|} - \frac{\exp(-\mu_t^*\|\mathbf{x}-\mathbf{x}_e\|)}{2\pi\|\mathbf{x}-\mathbf{x}_e\|^2}\right) \approx \sum_{e\in\Omega_{tip}} P^*(t)V_e\frac{3\mu_{tr}\exp(-\mu_{eff}\|\mathbf{x}-\mathbf{x}_e\|)}{4\pi\|\mathbf{x}-\mathbf{x}_e\|}$$

$$\mu_{eff}(\mathbf{x},m) = \sqrt{3\mu_a(\mathbf{x},m)\mu_{tr}(\mathbf{x},m)}$$

3 Wave Propagation

Computer models of the partial differential equation governing the propagation of the acoustic wave are expensive. Approximations using k-space methods and greens function techniques for back projection will be utilized....

4 User Interface

Example code and user interface is provided from the project site,
`https://github.com/ImageGuidedTherapyLab/PALikelihoodMap`. GPU kernels use a grid stride loop design pattern for compute intensive physics model calculations. The MATLAB script `exampleRecon.m` computes the wavelength sensitivity in two steps.

1. Uncertainty quantification techniques are applied to compute the variance of the photoacoustic source, Section 1 and Section 2.

2. Sensitivity statistics are propagated through our photo acoustic model for the wave propagation, Section 3.

The SDA fluence model is proportional to photoacoustic source, $S(r)\left[\frac{W}{m^3}\right]$, with a proportionality constant given by the *dimension-less* Gruneisen parameter, $\Gamma = \frac{v_s^2 \beta}{c_p}$

$$\text{PA source} = S(r) = \Gamma \mu_a \varphi_t \propto \sum_e P^*(t) V_e \frac{\mu_{eff}^2 \exp(-\mu_{eff}(\mathbf{x})\|\mathbf{x}-\mathbf{x}_e\|)}{4\pi\|\mathbf{x}-\mathbf{x}_e\|}$$

$$\mu_{eff} = \sqrt{3\mu_a\mu_{tr}} \quad \mu_{tr} = \mu_a + \mu_s(1-g)$$

$$\mu_a(\lambda, x) = \phi(x)\mu_a^{\text{HHb}}(\lambda) + (1-\phi(x))\mu_a^{\text{HbO2}}(\lambda)$$

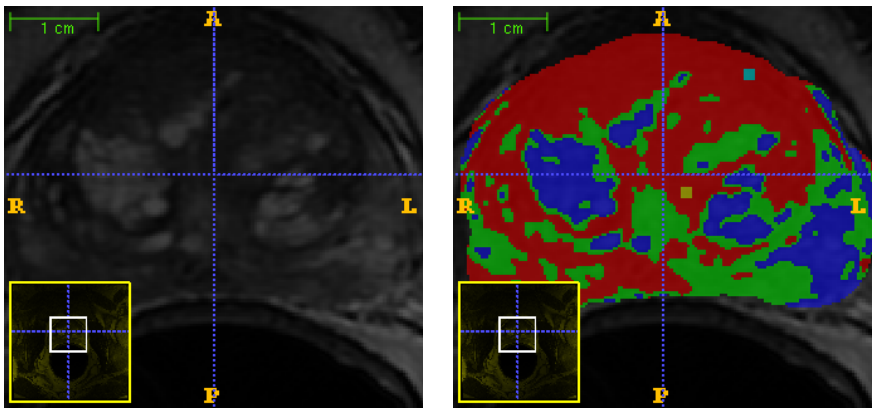

$$\Omega = \cup_j \Omega_j \qquad \Omega_i \cap \Omega_j = \emptyset \quad i \neq j \qquad \psi_j(x) = \begin{cases} 1 & x \in \Omega_j \\ 0 & x \notin \Omega_j \end{cases} \qquad \phi(x) = \sum_{j=1}^{N_\phi=3} \phi_j \psi_j(x)$$

Figure 1: The spatial decomposition is given by a three constituent Gaussian mixture model applied to pre-procedural imaging. The label map also encodes the laser applicator location (Label = 4 = applicator centroid, Label = 5 = entry point).

Assuming each parameter is independent, the parameter space probability function is the tensor product of the individual distributions.

$$\begin{aligned} \theta &= \left(\phi_1, ..., \phi_3, \mu_a^{\text{HHb}}(\lambda), \mu_a^{\text{HbO2}}(\lambda)\right) \\ \mu_a &= \left(\theta_1\psi_1(x) + \theta_2\psi_2(x) + \theta_3\psi_3(x)\right)\theta_4 \\ &\quad + \left(1 - \theta_1\psi_1(x) + \theta_2\psi_2(x) + \theta_3\psi_3(x)\right)\theta_5 \end{aligned} \qquad p(s|\theta) = \frac{1}{\sqrt{2\,\pi\,\Sigma_s}} \exp^{-\frac{(s-\Gamma\mu_a\varphi_t)^2}{2\,\Sigma_s}}$$

$$p(\theta) = \underbrace{1}_{\mathcal{U}(0,1)} \cdot \underbrace{1}_{\mathcal{U}(0,1)} \cdot \underbrace{1}_{\mathcal{U}(0,1)} \cdot \underbrace{\frac{1}{\sqrt{2\,\pi\,\Sigma_{\mu_a}}} \exp^{-\frac{(\theta_4 - \bar{\mu_a}^{\text{HHb}}(\lambda))^2}{2\,\Sigma_{\mu_a}}}}_{\mathcal{N}(\bar{\mu_a}^{\text{HHb}}(\lambda), \Sigma_{\mu_a})} \cdot \underbrace{\frac{1}{\sqrt{2\,\pi\,\Sigma_{\mu_a}}} \exp^{-\frac{(\theta_5 - \bar{\mu_a}^{\text{HbO2}}(\lambda))^2}{2\,\Sigma_{\mu_a}}}}_{\mathcal{N}(\bar{\mu_a}^{\text{HbO2}}(\lambda), \Sigma_{\mu_a})}$$

Table 1: Constitutive Data used in numerical simulations [Welch, 1984, Duck, 1990]

$\bar{\mu_a}^{\text{HHb}}(750nm)\ \frac{1}{m}$	$\bar{\mu_a}^{\text{HHb}}(850nm)\ \frac{1}{m}$	$\bar{\mu_a}^{\text{HbO2}}(750nm)\ \frac{1}{m}$	$\bar{\mu_a}^{\text{HbO2}}(850nm)\ \frac{1}{m}$	g	$\mu_s\ \frac{1}{cm}$	$\sqrt{\Sigma_{\mu_a}}\ \frac{1}{m}$	Γ
7.e2	4.e2	5.e2	6.e2	0.9	140.e2	1.e1	.45

Uncertainty quantification techniques [Fahrenholtz et al., 2013] are used to evaluate sensor model statistics.

$$\bar{S}(\lambda) = \mathbb{E}[S] = \int_S ds\ s \underbrace{\int_\theta d\theta\ p(s|\theta)\ p(\theta)}_{p(s)} \qquad \text{Var}(S)(\lambda) = \mathbb{E}[(S-\bar{S})^2] = \int_S ds\ (s-\bar{S})^2 \underbrace{\int_\theta d\theta\ p(s|\theta)\ p(\theta)}_{p(s)}$$

$$p(s) = \int_0^1 \int_0^1 \int_0^1 \int_{\mathbb{R}} \int_{\mathbb{R}} d\theta \; p(s|\theta) \; \frac{1}{\sqrt{2\,\pi\,\Sigma_{\mu_a}}} \exp^{-\frac{(\theta_4 - \bar{\mu_a}^{\mathrm{HHb}}(\lambda))^2}{2\,\Sigma_{\mu_a}}} \; \frac{1}{\sqrt{2\,\pi\,\Sigma_{\mu_a}}} \exp^{-\frac{(\theta_5 - \bar{\mu_a}^{\mathrm{HbO2}}(\lambda))^2}{2\,\Sigma_{\mu_a}}}$$

$$= \int_0^1 \int_0^1 \int_0^1 \int_{\mathbb{R}} \int_{\mathbb{R}} d\theta \; \frac{1}{\sqrt{2\,\pi\,\Sigma_s}} \exp^{-\frac{(s - \Gamma\mu_a(\theta)\varphi_t(\theta))^2}{2\,\Sigma_s}} \; \frac{1}{2\,\pi\,\Sigma_{\mu_a}} \exp^{-\frac{(\theta_4 - \bar{\mu_a}^{\mathrm{HHb}}(\lambda))^2 + (\theta_5 - \bar{\mu_a}^{\mathrm{HbO2}}(\lambda))^2}{2\,\Sigma_{\mu_a}}}$$

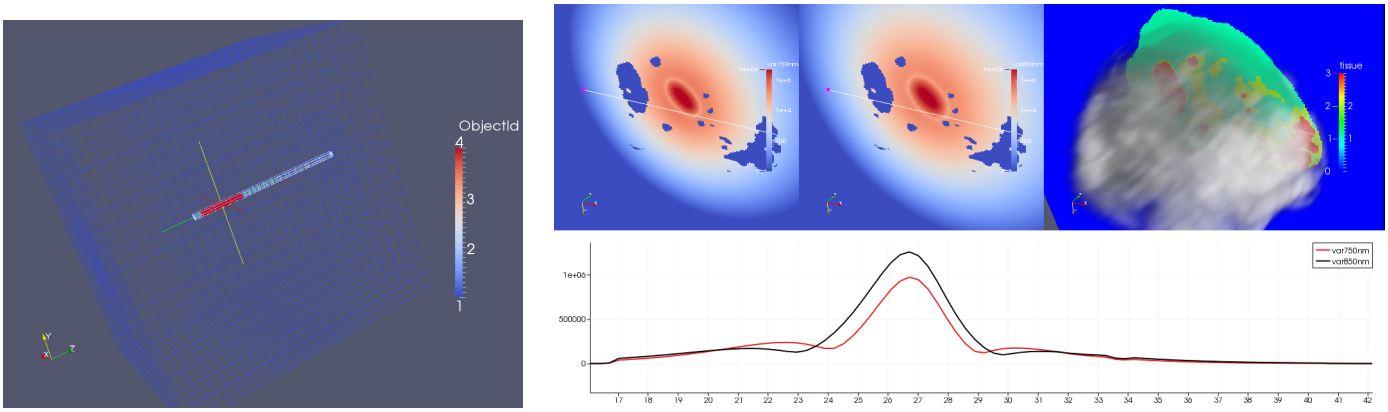

(a) (b)

Figure 2: Wavelength Sensitivity. (a) The model of the laser applicator is registered to the prostate data set shown in Figure 1. (b) The predicted sensitivity at $\lambda = 750nm$ and $\lambda = 850nm$ is shown. As expected the photoacoustic source is most sensitive, ie provides the most information near the laser fiber. Line profiles quantitatively compare the expected sensitivity with distance from the laser fiber as well as variations over distinct tissue types.

References

[Ahmed and Gokhale, 1989] Ahmed, N. A. and Gokhale, D. (1989). Entropy expressions and their estimators for multivariate distributions. *IEEE Transactions on Information Theory*, 35(3):688–692.

[Carp et al., 2004] Carp, S. A., Prahl, S. a., and Venugopalan, V. (2004). Radiative transport in the delta-P1 approximation: accuracy of fluence rate and optical penetration depth predictions in turbid semi-infinite media. *Journal of biomedical optics*, 9(3):632–47.

[Duck, 1990] Duck, F. (1990). Physical properties of tissue: a comprehensive reference book. *London, UK: Academic*.

[Durrett, 2010] Durrett, R. (2010). *Probability: theory and examples*. Cambridge university press.

[Fahrenholtz et al., 2015] Fahrenholtz, S., Moon, T., Franco, M., Medina, D., Hazle, J. D., Stafford, R. J., Maier, F., Danish, S., Gowda, A., Shetty, A., Warburton, T., and Fuentes, D. (2015). A Model Evaluation Study for Treatment Planning of Laser Induced Thermal Therapy. *International Journal of Hyperthermia*. in preparation.

[Fahrenholtz et al., 2013] Fahrenholtz, S., Stafford, R. J., Hazle, J., and Fuentes, D. (2013). Generalised polynomial chaos-based uncertainty quantification for planning MRgLITT procedures. *International Journal of Hyperthermia*, 29(4):324–335. PMC3924420.

[Fasano et al., 2010] Fasano, A., Hömberg, D., and Naumov, D. (2010). On a mathematical model for laser-induced thermotherapy. *Applied Mathematical Modelling*, 34(12):3831–3840.

[Fuentes et al., 2013] Fuentes, D., Elliott, A., Weinberg, J. S., Shetty, A., Hazle, J. D., and Stafford, R. J. (2013). An Inverse Problem Approach to Recovery of In-Vivo Nanoparticle Concentrations from Thermal Image Monitoring of MR-Guided Laser Induced Thermal Therapy. *Ann. BME.*, 41(1):100–111. PMC3524364.

[Fuentes et al., 2010] Fuentes, D., Feng, Y., Elliott, A., Shetty, A., McNichols, R. J., Oden, J. T., and Stafford, R. J. (2010). Adaptive Real-Time Bioheat Transfer Models for Computer Driven MR-guided Laser Induced Thermal Therapy. *IEEE Trans. Biomed. Eng.*, 57(5). Cover Page, PMC3857613.

[Fuentes et al., 2009] Fuentes, D., Oden, J. T., Diller, K. R., Hazle, J., Elliott, A., , Shetty, A., and Stafford, R. J. (2009). Computational Modeling and Real-Time Control of Patient-Specific Laser Treatment Cancer. *Ann. BME.*, 37(4):763. PMC4064943.

[Fuentes et al., 2011] Fuentes, D., Walker, C., Elliott, A., Shetty, A., Hazle, J., and Stafford, R. J. (2011). MR Temperature Imaging Validation of a Bioheat Transfer Model for LITT. *International Journal of Hyperthermia*, 27(5):453–464. Cover Page, PMC3930085.

[MacLellan et al., 2013] MacLellan, C. J., Fuentes, D., Elliott, A. M., Schwartz, J., Hazle, J. D., and Stafford, R. J. (2013). Estimating nanoparticle optical absorption with magnetic resonance temperature imaging and bioheat transfer simulation. *International Journal of Hyperthermia*, (0):1–9.

[Madankan et al., 2015] Madankan, R., Stefan, W., Hazle, J. D., Stafford, R. J., and Fuentes, D. (2015). Accelerated Model-based Signal Reconstruction for Magnetic Resonance Imaging in Presence of Uncertainties. *IEEE Trans. Med. Img.* submitted.

[Modest, 2013] Modest, M. F. (2013). *Radiative heat transfer*. Academic press.

[Stefan et al., 2015] Stefan, W., Fuentes, D., Yeniaras, E., Hwang, K., Hazle, J. D., and Stafford, R. J. (2015). Novel Method for Background Phase Removal on MRI Proton Resonance Frequency Measurements. *Trans. Medical Imaging*. in review.

[Welch, 1984] Welch, A. J. (1984). The thermal response of laser irradiated tissue. *Quantum Electronics, IEEE Journal of*, 20(12):1471–1481.

[Welch and Van Gemert, 1995] Welch, A. J. and Van Gemert, M. J. (1995). *Optical-thermal response of laser-irradiated tissue*, volume 1. Springer.

[Yung et al., 2015] Yung, J., Fuentes, D., MacLellan, C. J., Maier, F., Hazle, J. D., and Stafford, R. J. (2015). Referenceless Magnetic Resonance Temperature Imaging using Gaussian Process Modeling. *Medical Physics*. in review.